

Yiting Xie ; Yu Maw Htwe ; Jennifer Padgett ; Claudia Henschke ; David Yankelevitz ; Anthony P. Reeves; Automated aortic calcification detection in low-dose chest CT images. Proc. SPIE 9035, Medical Imaging 2014: Computer-Aided Diagnosis, 90350P (March 20, 2014);

doi:10.1117/12.2043810.

© (2014) COPYRIGHT Society of Photo-Optical Instrumentation Engineers (SPIE). Downloading of the paper is permitted for personal use only. Systematic or multiple reproduction, duplication of any material in this paper for a fee or for commercial purposes, or modification of the content of the paper are prohibited.

Automated aortic calcification detection in low-dose chest CT images

Yiting Xie^a, Yu Maw Htwe^b, Jennifer Padgett^a, Claudia Henschke^b, David Yankelevitz^b and Anthony P. Reeves^a

^aSchool of Electrical and Computer Engineering, Cornell University, Ithaca, NY, USA

^bDepartment of Radiology, Icahn School of Medicine at Mount Sinai, New York, NY, USA

Abstract

The extent of aortic calcification has been shown to be a risk indicator for vascular events including cardiac events. We have developed a fully automated computer algorithm to segment and measure aortic calcification in low-dose non-contrast, non-ECG gated, chest CT scans. The algorithm first segments the aorta using a pre-computed Anatomy Label Map (ALM). Then based on the segmented aorta, aortic calcification is detected and measured in terms of the Agatston score, mass score, and volume score. The automated scores are compared with reference scores obtained from manual markings.

For aorta segmentation, the aorta is modeled as a series of discrete overlapping cylinders and the aortic centerline is determined using a cylinder-tracking algorithm. Then the aortic surface location is detected using the centerline and a triangular mesh model. The segmented aorta is used as a mask for the detection of aortic calcification. For calcification detection, the image is first filtered, then an elevated threshold of 160 Hounsfield units (HU) is used within the aorta mask region to reduce the effect of noise in low-dose scans, and finally non-aortic calcification voxels (bony structures, calcification in other organs) are eliminated. The remaining candidates are considered as true aortic calcification.

The computer algorithm was evaluated on 45 low-dose non-contrast CT scans. Using linear regression, the automated Agatston score is 98.42% correlated with the reference Agatston score. The automated mass and volume score is respectively 98.46% and 98.28% correlated with the reference mass and volume score.

Keywords: aorta segmentation, aortic calcification measurement, automated computer algorithm, low-dose non-contrast CT

1. Introduction

Aortic calcification is a risk factor associated with various diseases. Thoracic aortic wall calcification is associated with hypertension [1], cerebral infarction [2], and other vascular diseases [3]. It is also closely associated with coronary calcification, cardiovascular events and death [4, 5]. Thus the automatic detection and measurement of thoracic aortic calcification can potentially aid physicians in the evaluation of coronary health.

Low-dose CT has become an accepted procedure in lung-cancer screening. Compared to standard-dose, low-dose CT exposes participants to much lower amounts of radiation [6]. I. Isgum et al performed aortic calcification scoring in low-dose non-contrast CT images using both manual and automatic Agatston scores and obtained a Spearman rank correlation coefficient of 96% [7]. This paper presents an alternative approach for automatic aortic calcification detection and quantification in low-dose non-contrast chest CT. The algorithm builds on a pre-computed anatomy label map (ALM), a robust chest segmentation infrastructure developed by the Cornell VIA group [15], and does not require manually marked training data in the development stage.

Compared to coronary calcification, aortic calcification usually has a very high Agatston score (AS). Coronary calcification with an AS greater than 400 is considered as severe while this would be considered as mild for aortic calcification. Figure 1 shows the 3D visualization of segmented aorta with calcification and their corresponding AS.

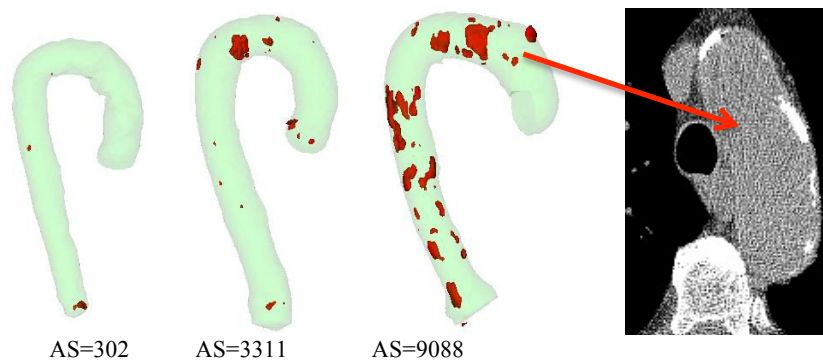


Figure 1. First three images: 3D visualization of segmented aorta (green) and aortic calcification (red) of 3 different cases and their respective Agatston score (AS). Last image is an axial slice of aortic arch with calcification and it corresponds to the 3rd visualization.

2. Methods

A previously developed aorta segmentation method [8] is used to segment the aorta region in a CT scan. The segmentation method makes extensive use of the original CT scan and its pre-computed Anatomy Label Map (ALM), which contains labels for pre-segmented anatomical entities including lungs, vertebrae, ribs, airways and fatty tissue [16]. For the ALMs used in this study: the airways were segmented using region growing based on a tree segmentation framework [10]; ribs were segmented using cylinder tracing and region growing [12]; lungs were segmented based on intensity threshold and the constraint from adjacent structures [13]. Together the segmented entities in the ALM provide a set of strong constraint to the location of the aorta.

To segment the aorta, first a seed point is determined within the aortic lumen at the level of the pre-segmented carina. Based on empirical observation, in this image slice the descending aorta is spatially bounded by left lung and vertebra and has a well-defined circular shape. A largest circle is fit into this unlabeled region and its center is the seed point (see figure 2).

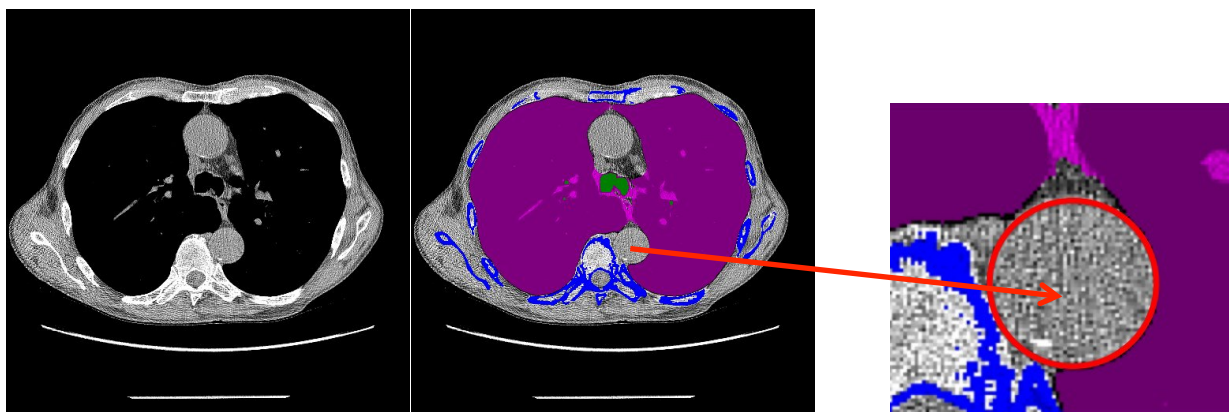


Figure 2. Illustration of seed point detection. From left to right: original image slice; its ALM with segmented entities in different colors: lung region in magenta, airway region in green and bone region in blue; largest circle in the empty region.

Starting from the seed point, the aorta is tracked in upward and downward directions. Tracking [9] is performed by iteratively fitting cylindrical sections to the unlabeled region in the ALM. In each iteration, candidate cylinders with different radii and orientations are generated (see figure 3(a)). The candidate with maximum unlabeled voxels and minimum labeled voxels is chosen as the best-fitting cylinder.

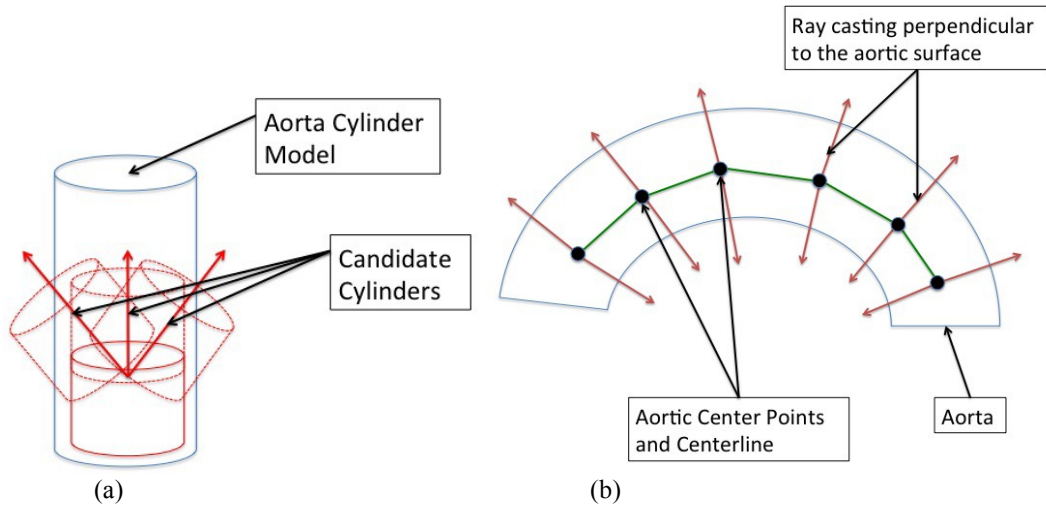


Figure 3. (a) aorta tracking model and candidate cylinders (b) aortic centerline and ray casting model.

Based on cylinder center points from tracking, a triangular mesh model adapted from [10] is used to detect the aortic surface location. Rays are projected perpendicular to the centerline towards the surface (see figure 3(b)). Each ray is filtered in the direction perpendicular to the aortic surface and traced until its intensity value falls to -30HU (tissue less dense than the aortic wall or the blood within the aortic lumen) or it intersects with an ALM labeled voxel. The termination point is the detected surface. All surface points are mapped back to the original image, resulting in the segmented aorta as shown in figure 4.

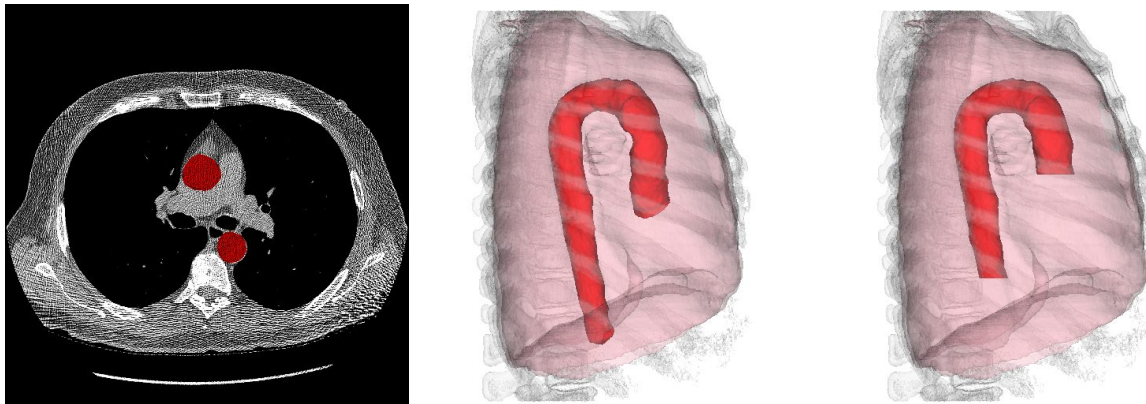


Figure 4. Left: original scan with segmented aorta (red) overlaid on it; middle: 3D visualization of segmented aorta (red) with lungs (light pink) and bone (light grey); right: 3D visualization of the same case with constrained aorta.

For the purpose of this experiment, the region of interest does not include aortic valve or the descending aorta below diaphragm. Therefore, the ascending aorta that extends into heart region and the descending aorta that extends beyond diaphragm is eliminated. The segmented aorta is used as a mask for the calcification detection.

It is standard practice to consider all voxels with an intensity value greater than 130HU in a region of interest as calcification. However, due to the high noise level in low-dose images, different criteria are used for the extraction of calcified candidates as follows:

- (1) The scan is first filtered with a filter $F=3 \times 3 \times 3$ mean.
- (2) In the aorta mask region, extract voxels with a HU value greater than threshold $I=160\text{HU}$. Then discard candidates with a size less than 5 voxels.

The selection of filter size and threshold value is a tradeoff between false positive and false negative voxels. In general, a larger filter size and a higher threshold value will result in more false negative calcification voxels and less false positive voxels while a smaller filter size and a lower threshold will result in more false positive and less false negative. Figure 5 and 6 show the effect of filter F and intensity I on calcification detection. It was observed that (1) with no filtering and standard threshold of 130HU, the majority of detected calcification is actually caused by image noise (figure 5 second image); (2) when filter size is too large (or threshold is too high) some true calcification voxels will be missed by the automatic algorithm (figure 5 last image). Figure 6 shows the effect of the elevated threshold on very noisy region: the original image has no calcification; using an elevated threshold of 160HU most of the false positive calcification is eliminated.

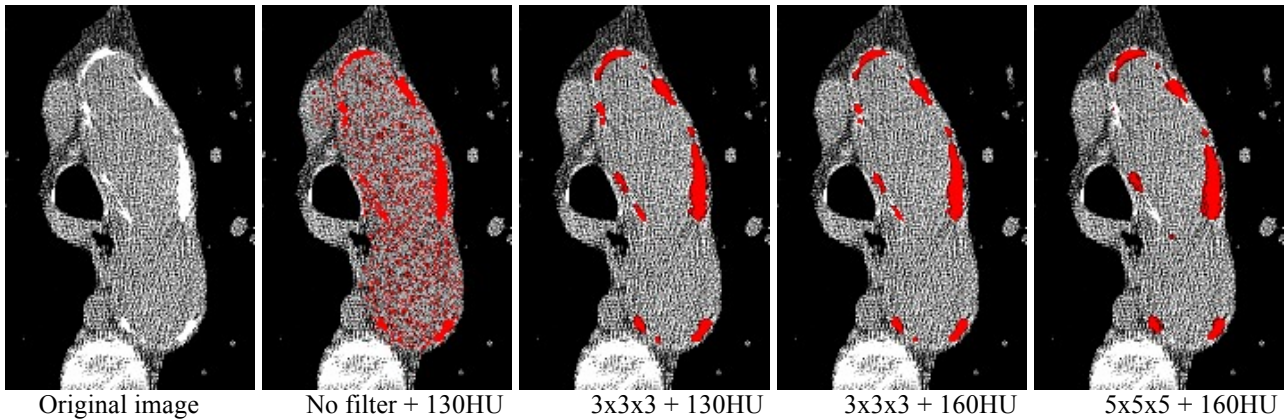


Figure 5. Illustration of filter size and threshold value on calcification detection. From left to right: first image is the original CT image; the other four images show the detected calcification (red) overlaid on the original image with different filter size and threshold. For example 3x3x3 + 130HU stands for 3x3x3 mean filter and a threshold of 130HU.

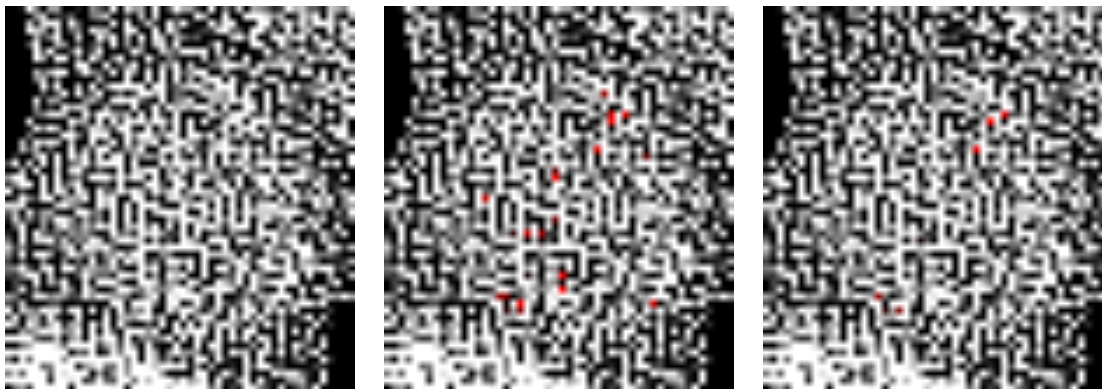


Figure 6. Effect of threshold on noisy descending aorta region. From left to right: original CT image; automatically detected calcification (red) overlaid on the original image using a threshold of 130HU and 160HU respectively. Both images have been filtered with a 3x3x3 mean filter.

The filter F and the elevation of threshold I are used to reduce the effect of noise in low-dose scans. Typically, the noise within the aortic lumen in low-dose scans is around 120HU. Without filtering, the majority of the calcified candidates are actually noise voxels. Similarly, if the standard threshold of 130HU is used, many noise voxels are classified as calcification.

After extraction of calcified candidates, using the pre-labeled ALM, candidates adjacent to the pre-segmented bony structures such as the vertebrae are considered as part of the bone and eliminated. Candidates adjacent to the pre-segmented airways are considered as airway calcification and eliminated as well (see figure 7). The remaining candidates are considered to be aortic calcification, based on which the Agatston score, mass score and volume score are computed.

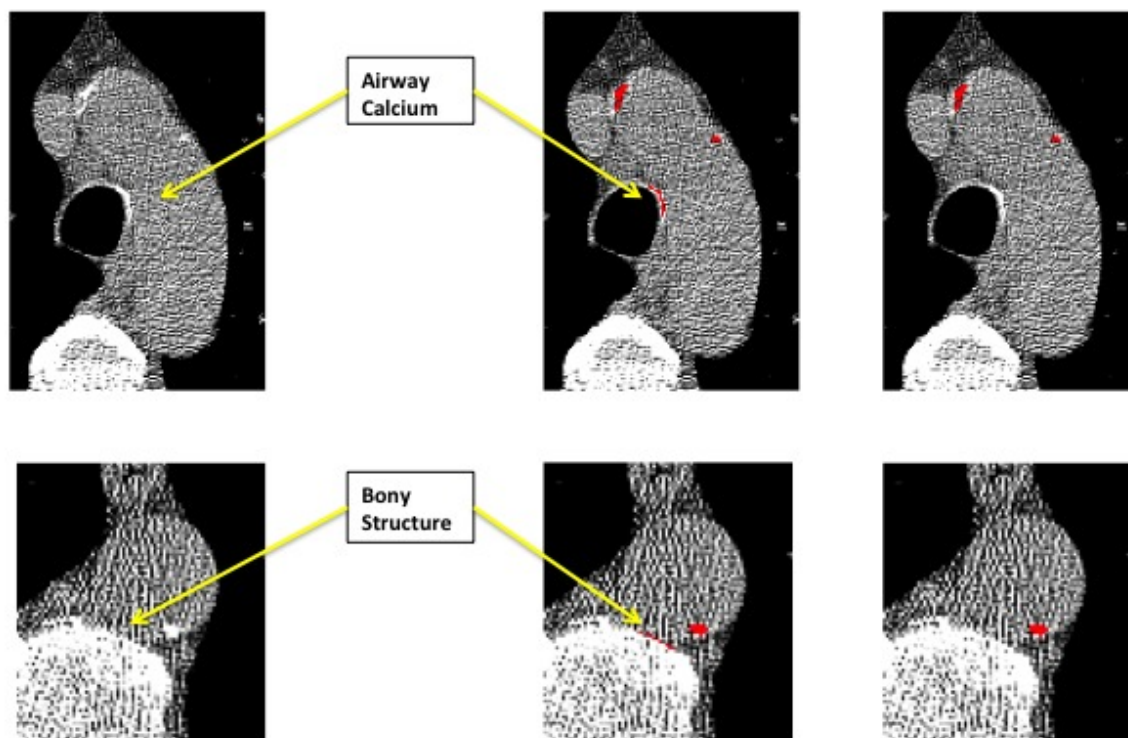


Figure 7. Elimination of airway calcification (top row) and bony structures (bottom row). From left to right: original image, selected calcium candidates (in red) before and after elimination of voxels adjacent to airway and bone.

3. Data and Results

In this study, 45 low-dose non-contrast non-ECG gated chest CT scans from the VIA-ELCAP [11, 14] database were used for evaluation. The automated scores are compared to their respective manual scores and the R-squared correlation coefficient based on linear regression is reported. Manual scores were obtained by filtering the image with a 3x3x3 mean filter and extracting voxels above 130HU in the manually marked regions. Since the manual markings only enclose the calcified regions, the standard threshold of 130HU was used to preserve as many calcified voxels as possible. This algorithm is designed for thoracic aortic calcification detection, thus aortic valve calcification and abdominal aortic calcification are excluded in both automated method and manual markings. Table 1 shows the R-squared correlation coefficient. Based on the automated Agatston score (AS), 34 (76%) cases had an AS greater than 400 and 22 (49%) cases had an AS greater than 1000.

Score	R-squared coefficient
Agatston Score	98.42%
Mass Score	98.46%
Volume Score	98.28%

Table 1. R-squared correlation coefficient between manual and automatic scores.

Figure 8 shows the AS histograms based on manual markings and the automated method. As there is no standard calcification level defined for aortic calcification, a specific level is defined in this paper. Level 1 to 4 respectively corresponds to an AS of [0, 400), [400, 1000), [1000, 5000), [5000, +∞). It is observed that there is only a slight difference between the distributions using manual and automatic methods.

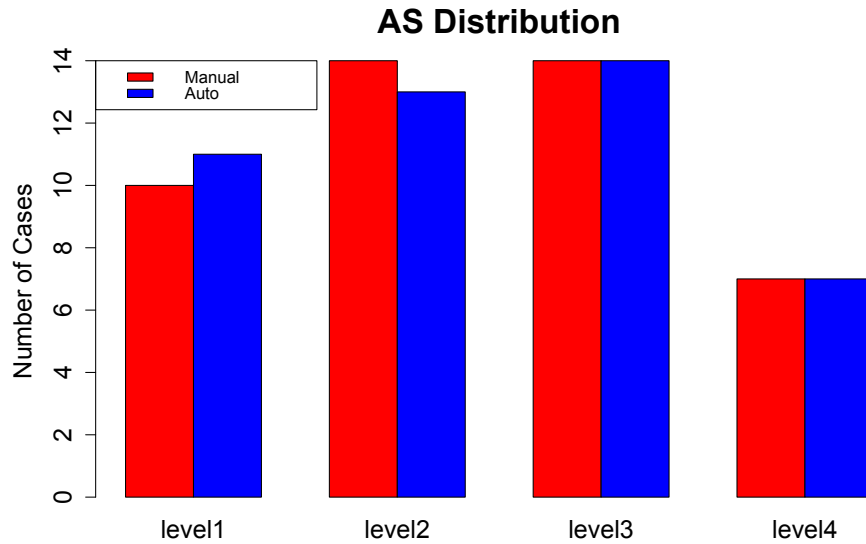


Figure 8. Histograms demonstrating the level of calcification based on AS from manual markings (red) and automatic detection (blue). x axis shows the calcification level (level1=[0, 400), level2=[400, 1000), level3=[1000, 5000), level4=[5000, +∞)) and y axis shows the number of cases.

Aortic arch calcification has been shown to be related to coronary heart disease in [4]. Based on visual inspection, it was also observed that in this dataset the aortic arch region in general contains more calcification compared to the ascending and descending regions. Therefore a second experiment was conducted to study the amount of calcification in different sections of aorta. As there is no standard definition for aortic arch region on CT images, in this experiment the aortic arch region is defined to be the section of aorta above the carina level (see figure 9). Figure 10 shows a histogram of calcification volume percentage for ascending, arch and descending sections respectively. The percentage is defined as: *number of calcified voxels in an aortic section / number of voxels in this section*. Level1 to level10 respectively corresponds to: [0, 0.05%), [0.05%, 0.1%), [0.1%, 0.15%), [0.15%, 0.2%), [0.2%, 0.3%), [0.3%, 0.4%), [0.4%, 0.5%), [0.5%, 1%), [1%, 1.5%), [1.5%, 5%). The levels were determined based on the distribution of aortic calcification. Since most regions only contain a very small percentage of calcification, most levels were assigned to below 1%. In this evaluation set, the maximum calcification volume percentage is less than 5%. From figure 10 it is observed that aortic arch in general contains more calcification compared to ascending and descending aorta. For the 45 cases in the test set, the average calcification volume percentage for aortic arch is 0.78%, versus 0.13% for ascending and 0.37% for descending aorta.

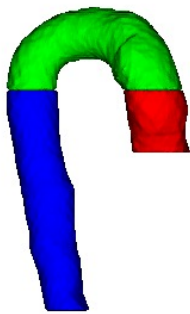


Figure 9. Illustration of aortic arch (green), ascending aorta (red) and descending aorta (blue).

Calcium Volume Percentage (%)

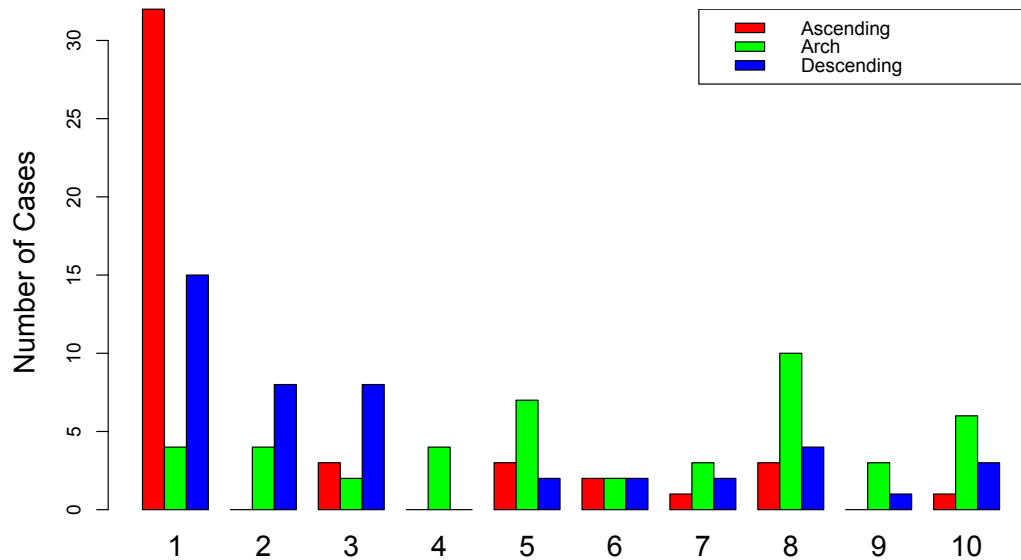


Figure 10. Calcification volume percentage histogram for ascending aorta (red), aortic arch (green) and descending aorta (blue). x axis shows the percentage level (bin1 = [0, 0.05%), bin2 = [0.05%, 0.1%), bin3 = [0.1%, 0.15%), bin4 = [0.15%, 0.2%), bin5 = [0.2%, 0.3%), bin6 = [0.3%, 0.4%), bin7 = [0.4%, 0.5%), bin8 = [0.5%, 1%), bin9 = [1%, 1.5%), bin10 = [1.5%, 5%)) and y axis shows the number of cases.

4. Discussion

In general, the automated algorithm is able to accurately detect calcified voxels. Disagreement between the automatic and manual method occurs as to the location of the diaphragm and the superior margin of the heart. These two locations are used to constrain aorta segmentation (see figure 11). However, the difference between the two methods is usually very small and does not have a major impact on the calcification evaluation.

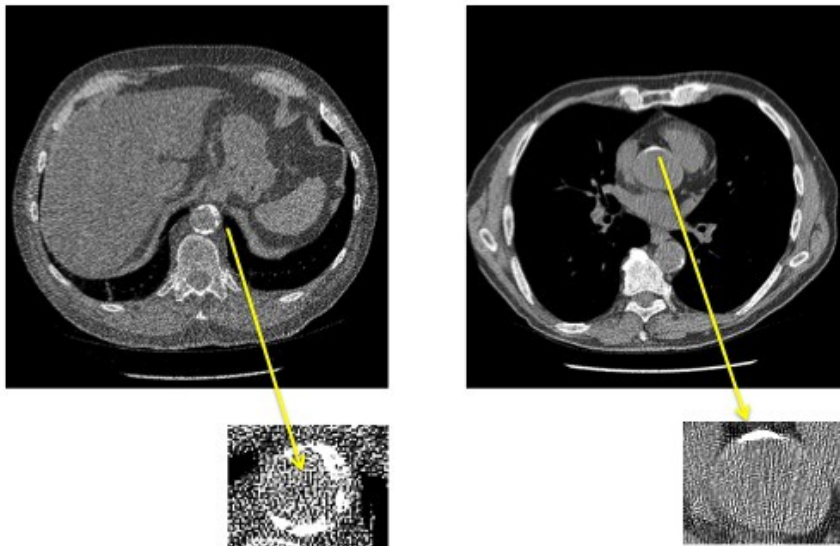


Figure 11. Missed calcification by automatic algorithm compared to manual markings. Left shows missed calcium close to the diaphragm region; right shows missed calcium close to the superior region of the heart.

5. Conclusion

We have developed an automated algorithm to segment and measure aortic calcification in low-dose non-contrast CT scans. The algorithm builds on a pre-labeled anatomy map. Filtering and an elevated threshold are used to reduce the effect of noise. Results show that the automatically measured Agatston score is 98.42% correlated with the Agatston score obtained from manual markings. The automatic volume and mass score is 98.28% and 98.46% correlated with the manual volume and mass score respectively. It has also been observed that in the evaluation set, aortic arch region on average contains more calcification based on volume percentage.

ACKNOWLEDGMENT

This study was supported by a grant from the Flight Attendant Medical Research Institute (FAMRI).

REFERENCES

- [1] Takasu, J., et al. "Relationships of thoracic aortic wall calcification to cardiovascular risk factors: The multi-ethnic study of atherosclerosis (MESA)." *Am. Heart J.* 155(4), 765-771 (2008).
- [2] Itani, Y., Watanabe, S., and Masuda, Y., "Relationship between aortic calcification and stroke in a mass screening program using a mobile helical computed tomography unit." *Jpn. Circ. J.* 70(6), 733-736 (2006).
- [3] Jacobs, P. C., et al. "Comparing coronary artery calcium and thoracic aorta calcium for prediction of all-cause mortality and cardiovascular events on low-dose non-gated computed tomography in a high-risk population of heavy smokers." *Atherosclerosis*. 209(2), 455-462 (2010).
- [4] Iribarren, C., Sidney, S., Sternfeld, B., and Browner, W. S., "Calcification of the aortic arch: Risk factors and association with coronary heart disease, stroke and peripheral vascular disease." *J. Am. Med. Assoc.* 283(21), 2810-2815 (2000).
- [5] Eisen, A., et al. "Calcification of the thoracic aorta as detected by spiral computed tomography among stable angina pectoris patients: Association with cardiovascular events and death." *Circulation* 118(13), 1328-1334 (2008).
- [6] McCollough, C. H., Bruesewitz, M. R., and Kofler, J. M., Jr, "CT Dose Reduction and Dose Management Tools: Overview of Available Options." *RadioGraphics* 26(2), 503-512 (2006).
- [7] Isgum, I., et al. "Automated aortic calcium scoring on low-dose chest computed tomography." *Med. Phys.* 37(2), 714-724 (2010).
- [8] Xie, Y., Padgett, J., Biancardi, A. M., and Reeves, A. P., "Automated aorta segmentation in low-dose chest CT images." *IJCARS* (2013).
- [9] Fotin, S. V., Reeves, A. P., Cham, M. D., Henschke, C. I., and Yankelevitz, D. F., "Segmentation of coronary arteries from CT angiography images." *SPIE Medical Imaging*. 651418—1 (2007).
- [10] Lee, J., Reeves, A. P., Fotin, S. V., Apanasovich, T., and Yankelevitz, D. F., "Human airway measurement from CT images." *SPIE Medical Imaging*. 691518 (2008).
- [11] ELCAP Public Lung Image Database. 13 May 2013 <www.via.cornell.edu/databases/lungdb.html>.
- [12] Lee, J. and Reeves, A. P., "Segmentation of individual ribs from low-dose chest CT." *SPIE Medical Imaging*. 7624, 762433J (2010).
- [13] Reeves, A. P., Chan, A. B., Yankelevitz, D. F., Henschke, C. I., Kressler, B. and Kostis, W. J., "On measuring the change in size of pulmonary nodules." *IEEE Trans. on Medical Imaging*. 25(4), 435-450 (2006).
- [14] Reeves, A. P., Biancardi, A. M., Yankelevitz, D. F., Fotin, S., Keller, B. M., Jiraptnakul, A. and Lee, J., "A Public Image Database to Support Research in Computer Aided Diagnosis." 31st Conf. IEEE EMBS. 3715-3718 (2009).
- [15] *Vision and Image Analysis Group, Cornell University*. 13 May 2013 <www.via.cornell.edu>.
- [16] Padgett, J., Biancardi, A. M., Henschke, C. I., Yankelevitz, D. and Reeves, A. P., "Local noise estimation in low-dose chest CT images." *IJCARS* (2013).